DEVELOPMENT OF THE MATRA-LMR-FB FOR FLOW BLOCKAGE ANALYSIS IN A LMR

KWI-SEOK HA*, HAE-YONG JEONG, WON-PYO CHANG, YOUNG-MIN KWON, CHUNGHO CHO and YONG-BUM LEE
Korea Atomic Energy Research Institute
150 Deokjin-dong, Yuseong-gu, Daejeon, 305-353 Korea
*Corresponding author. E-mail : ksha@kaeri.re.kr

Received October 13, 2008
Accepted for Publication February 12, 2009

The Multichannel Analyzer for Transient and steady-state in Rod Array - Liquid Metal Reactor for Flow Blockage analysis (MATRA-LMR-FB) code for the analysis of a subchannel blockage has been developed and evaluated through several experiments. The current version of the code is improved here by the implementation of a distributed resistance model which accurately considers the effect of flow resistance on wire spacers, by the addition of a turbulent mixing model, and by the application of a hybrid scheme for low flow regions. Validation calculations for the MATRA-LMR-FB code were performed for Oak Ridge National Laboratory (ORNL) 19-pin tests with wire spacers and Karlsruhe 169-pin tests with grid spacers. The analysis of the ORNL 19-pin tests conducted using the code reveals that the code has sufficient predictive accuracy, within a range of 5 °C, for the experimental data with a blockage. As for the results of the analyses, the standard deviation for the Karlsruhe 169-pin tests, 0.316, was larger than the standard deviation for the ORNL 19-pin tests, 0.047.

KEYWORDS : Sub-channel, Blockage, LMR, Distributed Resistance Model, MATRA-LMR

1. INTRODUCTION

A sodium-cooled fast reactor has a compact arrangement of fuel rods with a high power density achieved through using a high energy neutron spectrum with a short prompt-neutron life time and a greater ease to supercritical conditions. These characteristics can threaten the safety of the reactor by increasing the fuel and coolant temperatures when a subchannel is blocked. The obstacles entering a subchannel or generated by a degraded fuel rod will increase the pressure drop and reduce the flow rate, and may cause fuel pin damage due to a reduced local cooling capability. To prevent or mitigate a serious accident, it is necessary to predict the temperature distributions within an assembly containing a flow blockage channel using a reliable computer code applicable to the situation.

The Multichannel Analyzer for Transient and steady-state in Rod Array - Liquid Metal Reactor (MATRA-LMR) [1], a subchannel analysis code, has been developed for the analysis of the thermal-hydraulics of a Liquid Metal-cooled Reactor (LMR) core where the design limits are imposed on the maximum temperatures of the cladding and fuel pins. The code is based on the COBRA-IVi code [2]. The code solves the governing equations for mass, momentum, and energy as a boundary problem in space and as an initial value problem in time.

The wire spacers in a LMR are helically wrapped around the rods to maintain the cooling geometry and to prevent the fuel rods from contacting an adjacent rod. Another role of the wire spacers is to enhance the coolant mixing by generating a swirl flow at the outer region of an assembly. When there is a blockage in a flow path, various flow fields are formed due to the wire spacers and the blockage. Therefore, an analysis code for a flow blockage requires a proper numerical scheme and a thermal hydraulic model to deal with these flow fields. To construct such a code, the MATRA-LMR-FB code has been developed by implementing a distributed resistance model (DRM) [3], a hybrid difference scheme [4], and a proper turbulent mixing model [5-9] into the MATRA-LMR.

Countries leading in the development of LMRs have performed extensive experimental research into flow blockages because of the importance of such blockages to the core safety of LMRs. The MATRA-LMR-FB code has been evaluated by using the experimental data from the ORNL 19-pin fuel failure mockup (FFM) bundle tests with wire spacers and the Karlsruhe data collected at the Karlsruhe Nuclear Research Centre (KfK) in experiments conducted with honeycomb grid spacers.

2. THE MODELING OF A FLOW BLOCKAGE

The MATRA-LMR code has two numerical schemes. One is a fully implicit method using a MARCHING scheme for solving the governing equations sequentially in the axial direction, and the other is an explicit method using an Implicit Continuous-fluid Eulerian (ICE) approach with an upwind scheme. The fully implicit method cannot model a reverse flow in the downstream of a blockage due to the characteristics of the MARCHING scheme. Thus, based on the explicit method, the DRM model has been implemented into the MATRA-LMR. The donor cell method for the convective terms in the MATRA-LMR code results in a significant numerical diffusion in the regions of a low flow and results in sharp gradients across a mesh such as the recirculating wakes after a blockage. To reduce this numerical diffusion, the numerical process for the convective terms has been modified to use an upwind scheme or a central scheme depending on the Reynolds number in the momentum equation and the Peclet number in the energy equations. To enhance the predictability of the flow and temperature distributions in the subchannels and to exclude a user dependency, various turbulent mixing models have been evaluated and implemented into the MATRA-LMR code.

2.1 Distributed Resistance Model

In the traditional subchannel analysis codes, and even in some recently developed subchannel codes such as MATRA-LMR, the transverse momentum equation is only used to solve the pressure variable and to estimate the initial conditions for the given time step. The transverse mass flow rate is given in proportion to the axial flow rate by assuming that the total flow rate is formed along the path of a wire spacer. In the model, the flow is locally redirected along the path of the wire spacer and the axial friction factor is distributed uniformly everywhere. Apparently, the model is only based on the consideration of mass conservation and does not account for the momentum effects. For a more detailed description of a wire spacer, the following DRM model has been implemented into the MATRA-LMR. The axial and transverse momentum balance equations of MATRA-LMR are written as follows:

$$\frac{\partial}{\partial t}\langle \rho u\rangle_V A+\frac{\partial}{\partial X}\langle \rho u^2\rangle_A A+\{D_C^T\}\langle \rho uv\rangle_S S= -A\frac{\partial}{\partial X}\langle p\rangle_A - A\langle \rho\rangle_A g - C_T\{D_C^T\}[w'][D_C]\{u'\}-\frac{1}{2}\left(\frac{f}{D_h}+\frac{K}{\Delta X}\right)\langle \rho u^2\rangle_A A \quad (1)$$

$$\frac{\partial}{\partial t}\langle \rho v\rangle_{V'} S+\frac{\partial}{\partial X}\langle \rho vu\rangle_{A'} S + C_S\{D_C\}\{D_C^T\}\left\{\frac{S}{l}\langle \rho v^2\rangle_S \cos\beta\right\} = -\frac{S}{l}\{D_C\}\{\langle p\rangle_A\}-\frac{1}{2}\frac{S}{l}K_G\langle \rho v^2\rangle_S \quad (2)$$

where β is the angle of a communicating gap and the gap of interest.

The last terms on the right-hand side of Eq. (1) and of Eq. (2) represent the momentum exchange between a solid surface and a fluid due to the forces exerted on the fluid by a wall such as the fuel rods and the wire spacers. To account for the presence of a wire spacer in a rod bundle and to represent the direction and resistance characteristics correctly, Davis et al. [4] developed the distributed resistance model for the SABRE (Subchannel Analysis of Blockage in Reactor Element) code. This model is applicable for the predominantly axial flows under turbulent flow conditions. Recently, Ninokata et al. [3] extended the model to predominantly lateral flows including laminar conditions, which is important for the modeling of a flow blockage because recirculating wakes are induced downstream from a blockage and the flow characteristics change drastically from a forced convection to a mixed convection.

The forces exerted on the fluid in the axial and transverse directions in the rod bundles with a wire spacer can be divided into four components as shown in Fig. 1. The details of the forces are well established in a study by Ha et al. [10]. The final forms of the distributed resistance of a wire spacer are as follows:

$$\frac{1}{2}\left(\frac{f}{D_h}+\frac{K}{\Delta X}\right)\langle \rho u^2\rangle_A A = \frac{1}{\Delta X}\left\{\frac{A_R f}{8}\rho c|c|\cos\theta+\frac{A_W f}{8}\rho c|c|\cos(\phi-\theta)\cos\phi+F_W^N\sin\phi\right\} \quad (3)$$

$$\frac{1}{2}\frac{S}{l}K_G\langle \rho v^2\rangle_S = \frac{1}{l\Delta X}\left\{F_R^L+\frac{A_W f}{8}\rho c|c|\cos(\phi-\theta)\sin\phi-F_W^N\cos\phi\right\} \quad (4)$$

- Predominantly lateral flow

$$F_R^L=\frac{A_R f}{8}\rho v|v|\left(\frac{D_V''}{S_T}\right)^{0.4}\left(\frac{S_L}{S_T}\right)^{0.6}\frac{1}{E(\omega)} \quad (5)$$

$$F_W^N=\frac{A_W f}{8}\rho v_N|v_N|\left(\frac{D_V''}{S_T}\right)^{0.4}\left(\frac{S_L}{S_T}\right)^{0.6}\frac{1}{E(\omega)} \quad (6)$$

- Predominantly axial flow

$$F_R^L=\frac{A_W'' f}{8}\rho v|v|\left(\frac{D_V''}{S_T}\right)^{0.4}\left(\frac{S_L}{S_T}\right)^{0.6} \quad (7)$$

$$F_W^N=\frac{A_{wp} f_n}{2}\rho v_N|v_N| \quad (8)$$

where the forces of F_R^L and F_W^N are estimated by different correlations according to the direction of a dominant flow as in Eqs. (5) ~ (8). A_R, A_W, and A_W'' are the surface area of

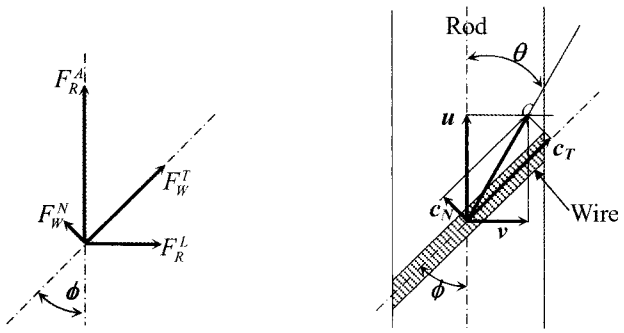

Fig. 1. Components of Drag Forces and Velocities in a Wire-wrapped Rod

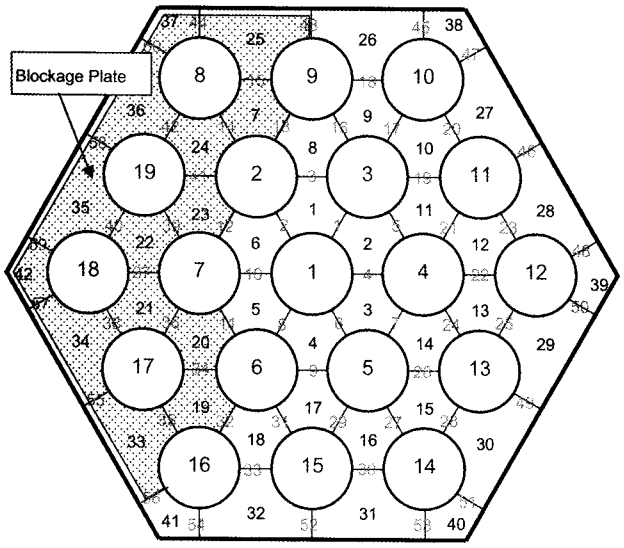

Fig. 2. Nodalization for the Simulation of ORNL 19-pin Test

the rod, the surface area of the wire-wrap, and the total surface area in a control volume, respectively. The "f"s means the friction factor, which is estimated using the appropriate correlations. In the case of lateral flow, the Gunter-Shaw correlation has been introduced with a multiplication factor $E(\omega)$ given by Suh et al. [11]. D_V'' is the volume-averaged hydrodynamic diameter, $D_V''= 4\Delta V_f/A_W''\cdot v_N$, which is defined as $v_N = u \sin\phi - v \cos\phi$, is the normal velocity on the wire-wrap direction. S_T is the rod pitch and S_L is the distance between the two rods in a transverse row (Fig. 2). A_{wp} is the frontal area of the wire-wrap. The first term of Eq. (3) means F_R^A and the second term represents the axial component of F_W^T in Fig. 1. The second term of Eq. (4) means the horizontal component of F_W^T. The right-hand sides of Eqs. (3) and (4) have been implemented into the MATRA-LMR code.

2.2 Hybrid Difference Scheme

The explicit scheme of the MATRA-LMR code basically adopts the upwind method to deal with the convection terms on a staggered grid. With the upwind method, the convective scalar properties such as the pressure, density, and temperature are determined depending on the direction of the velocity at the boundary of the control volume. The upwind differencing is known to enhance the numerical stability but it induces a numerical diffusion in the case of sharp gradients across a computational grid. In addition, the resultant numerical diffusion is inversely proportional to the convective velocity. That is, while a high velocity diminishes a numerical diffusion, a low velocity increases it. When a blockage is formed in a rod bundle, the flow fields spread from a Stokes flow to a turbulent flow through a laminar region. Thus, if the upwind differencing is applied for the whole flow region with a blockage, a large numerical diffusion is unavoidable in a low flow region and for sharp gradients across a mesh such as the recirculating wakes after a blockage.

Central differencing drastically reduces the numerical diffusion in a low flow region [12]. To avoid an unphysical numerical diffusion in the analysis of a flow blockage, the hybrid differencing scheme is applied depending on the Reynolds (Re) number and the Peclet (Pe) number. Central differencing is used when the Reynolds number is less than 2 or the Peclet number is less than 2. With hybrid differencing, the convective terms in the axial momentum equation, the transverse momentum equation, and the energy equation are respectively expressed as follows:

$$u\frac{\partial m}{\partial x} = \begin{cases} \frac{1}{\Delta x}\left[\left(um^*\right)_{j+1} - \left(um^*\right)_j\right] & \text{if } \mathrm{Re} \geq 2 \\ \frac{1}{\Delta x}\left[\frac{1}{2}\left(m^*_{j+1} + m^*_j\right)\left(u_{j+1} - u_j\right)\right] & \text{if } \mathrm{Re} < 2 \end{cases} \quad (9)$$

$$\bar{u}\frac{\partial w}{\partial y} = \begin{cases} \frac{1}{\Delta x}\left[\left(\bar{u}w^*\right)_k - \left(\bar{u}w^*\right)_l\right] & \text{if } \mathrm{Re} \geq 2 \\ \frac{1}{\Delta y}\left[\frac{1}{2}\left(w^*_k + w^*_l\right)\left(\bar{u}_k - \bar{u}_l\right)\right] & \text{if } \mathrm{Re} < 2 \end{cases} \quad (10)$$

$$V\frac{\partial(\rho uh)}{\partial z} = \begin{cases} \left[\left(mh^*\right)_{j+1} - \left(mh^*\right)_j\right] & \text{if } \mathrm{Pe} \geq 2 \\ \left[\frac{1}{2}\left(h^*_{j+1} + h^*_j\right)\left(m_{j+1} - m_j\right)\right] & \text{if } \mathrm{Pe} < 2 \end{cases} \quad (11)$$

where the superscript '*' and bar mean the donor properties and the averaged value between adjacent nodes, and the subscripts j, k, l are the node indices.

2.3 Turbulent Mixing Model

When a single phase fluid is flowing in subchannels, the mixing of the mass, energy, and momentum between subchannels can be divided into two parts: the mixing by the diversion flow due to the pressure gradient and the mixing by the cross flow mainly due to the turbulent

effect. MATRA-LMR models the inter-subchannel mixing phenomenon based on a fluctuating equal mass exchange. The effects of turbulent mixing in the code are considered in the axial momentum equation and the energy equation.

The third term on the right-hand side of Eq. (1) represents the contribution of the turbulent mixing between the subchannel of interest and its adjacent subchannels. The turbulent mixing flow rate through an interface of subchannels is defined using a turbulent mixing coefficient, η, as follows:

$$w' = \eta S \bar{G} \tag{12}$$

where S is the gap width and $\bar{G}$ is the average axial mass flux flowing along the subchannels. The mixing coefficient is essentially the same as the gap Stanton number, $St_g=\eta$. The turbulent mixing coefficient is normally determined from the thermal mixing test at single phase conditions. It is evaluated with the following equation from the diffusive energy flux between the subchannels:

$$\eta = \frac{\varepsilon_H}{l}\frac{\bar{\rho}}{\bar{G}} \tag{13}$$

where l is the distance between the centers of two adjacent subchannels. In the MATRA-LMR, the turbulent mixing coefficient is directly input by a code user. The main shortcoming of the model is the lack of a physical basis for selecting a constant value for the mixing coefficient. Further, in the analysis of a flow blockage, a constant mixing coefficient does not reflect the various degrees of mixing, which are dependent on flow regimes ranging from a stagnant flow to a fully developed turbulent flow. Using the above model for turbulent mixing, the magnitude of mixing in the recirculating wake region due to a flow blockage can be differed because it has a constant mixing coefficient. The mixing coefficient is essentially the same as the gap Stanton number St_g, and therefore we investigated several turbulent mixing models [5-8]. The model suggested by Kim and Chung [5] was finally implemented into the MATRA-LMR code. The original turbulent mixing model from Kim and Chung is composed of molecular motion, isotropic turbulent motion, and flow pulsation; however, the term for molecular motion is the same as the conduction equation for the conductive heat transfer through the fluid itself, which is separately modeled in a subchannel energy equation. As a result, the pure turbulent mixing containing mixing due to isotropic turbulence and mixing from a flow pulsation of Eq. (14) was used [13].

$$St_g = \frac{2}{\gamma^2}\sqrt{\frac{\alpha}{8}}\frac{D_h}{S}\left[\frac{1}{\mathrm{Pr}_t}\frac{S}{b\cdot l} + a_x\frac{z_{FP}}{d}\mathrm{Str}\right]\mathrm{Re}^{-\beta/2} \tag{14}$$

where α and β are the constants for the friction factor expressed as $f=\alpha\,\mathrm{Re}^{-\beta}$, and γ is an empirical constant. In Eq. 14, Pr_t is the turbulent Prandtl number, Str is the Strouhal's number, d is the rod diameter, z_{FP} is the hypothetical path length of a flow pulsation, a_x is the directional velocity scale of a flow pulsation, and b is the shape factor for the length scale for a transverse flow pulsation. The value of Eq. (14) ranged from 0.0015 to 0.0069 depending on the thermal hydraulic conditions of the calculated control volume in a simulation of the ORNL high flow test.

3. SIMULATION RESULTS FOR A FLOW BLOCKAGE

The effects of the models described in Section 2 were evaluated by JEONG et al. The ORNL 19-pin tests [14, 15] performed with wire spacers and the Karlsruhe 169-pin tests [16] performed with grid spacers and conducted at the Karlsruhe Nuclear Research Centre were used to validate the developed MATRA-LMR-FB code as shown in Table 1. Two ORNL tests without a blockage (FFM-2A) and two ORNL tests with a blockage (FFM-5B) with different flow rates and heat fluxes were selected for the wire spacer. Each of the 19 fuel rods has a diameter of 5.842 mm and all the rods are arranged in a triangular

Table 1. Boundary Conditions of the Experimental Tests

Paramerter	ORNL 19-pin tests				Karlsruhe 169-pin tests			
	FFM-2A		FFM-5B		49 % Central Blockage		21 % Corner Blockage	
Inlet temperature, °C	315.0	315.0	323.6	268.4	404.0	404.0	397	395
Inlet velocity, m/s	7.16	0.10	6.93	0.48	4	1	1	4
Heat flux, W/cm^2	173.50	2.68	90.95	33.12	67.7	17.9	30.1	111.3
Re	>35000	>450	>30000	>2500	>17000	>4000	>4000	>17000
Pe	>195	>2.7	>160	>18	>90	>23	>23	>90

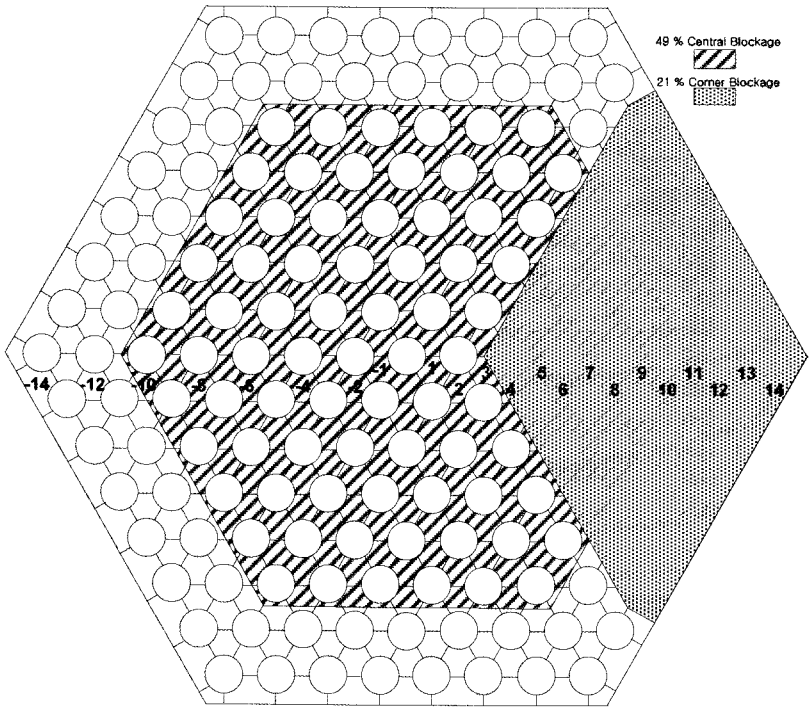

Fig. 3. Nodalization for the Simulation of KfK 169-pin Test

pitch within a hexagonal duct. Spacing between the rods is maintained by a wire wrapped helically around each rod. The wire spacers have a diameter of 1.4224 mm in the central region and there is 0.7112 mm between each rod and the duct wall. As the liquid sodium flows upward through the test section, it first passes through an entrance region of 304.8 mm, then a heated section of 533.4 mm, and finally an exit region where thermocouples measure the outlet temperature distribution across the duct. The blockage plate is positioned 406.4 mm from the inlet. The wire spacer wraps around the rod counter-clockwise as it moves up the rod and its pitch is 304.8 mm. A schematic diagram for the simulation of the experiments is given in Fig. 2. The test assembly was modeled with 40 subchannels, 60 gaps, and 40 axial levels each with a length of 25.4 mm.

The 49 % central blockage test and the 21 % corner blockage test of the Karlsruhe experiments were chosen for the honeycomb grid spacer. The pin diameter and pitch are 6 mm and 7.9 mm, respectively. The blockage plate has a 3mm thickness incorporated in a spacer grid 40 mm downstream from the start of the heated length. The grid spacers are arranged with a 150 mm span from the inlet to the start of the heated part and the heated length is 290 mm. Only 88 pins in the blocked part of the 169 pins in the test with the 49 % blockage are heated and the remaining pins are unheated dummies. In the test with the 21 % corner blockage, the blocked area is surrounded by 3 rows of heaters. The test section was modeled with 342 subchannels, 510 gaps, and 74 axial levels, as shown in Fig. 3. The total flow length of 1,016 mm was nodalized into 74 axial volumes. The tests were carried out for the inlet velocities of 1 m/s and 4 m/s. The boundary conditions and the non-dimensional numbers of the Re number and Pe number for these simulations are summarized in Table 1.

The simulation results by MATRA-LMR-FB for the ORNL tests are depicted in Figs. 4 ~ 7. In the case of the tests without a blockage, the large temperature gradients at the edge and outer regions are formed because of the swirl flow at the edge, which is a representative characteristic of a wire-wrapped channel. The calculation results agree well with the results of the experiments conducted without a blockage, falling in the range of about 10 °, as shown in Fig. 4 and Fig. 5.

The prediction capability of the MATRA-LMR-FB code for a flow blockage analysis was assessed by using the experiments conducted in the FFM-5B test bundle. In the experiments in the test bundle, about one third of the flow area is blocked at the edge around the corner subchannels, marked as 37, 42 and 41 in Fig. 2. When a certain part of the flow path is blocked, the downstream temperature of the blockage increases, as shown by the experimental data in Fig. 6 and Fig. 7. This mainly results from the formation of recirculating wakes just above the blockage. In Fig. 6, it can also be seen that the temperature

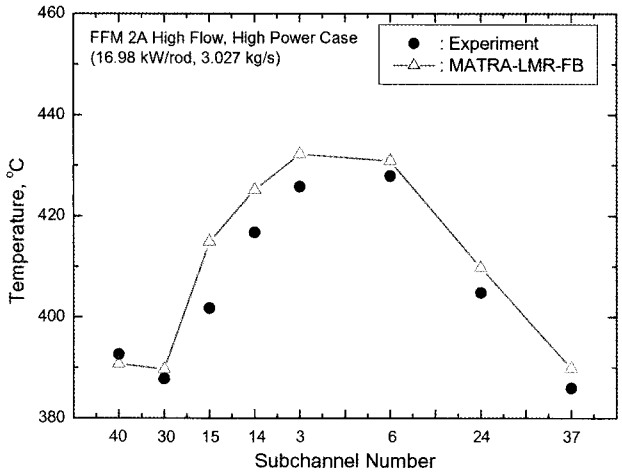

Fig. 4. The Calculation Results for ORNL High Flow Test without Blockage at Exit Region

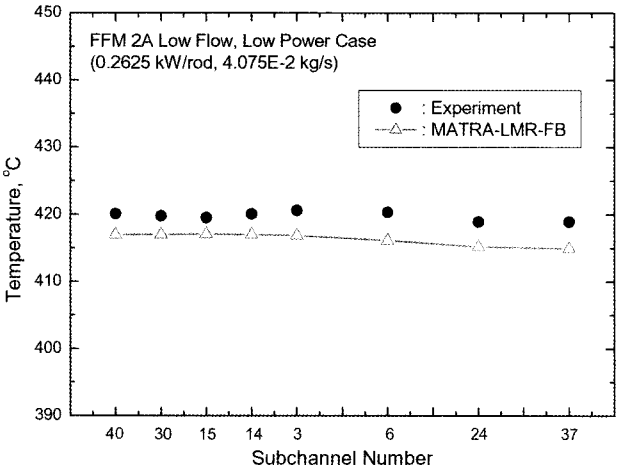

Fig. 5. The Calculation Results for ORNL Low Flow Test without Blockage at Exit Region

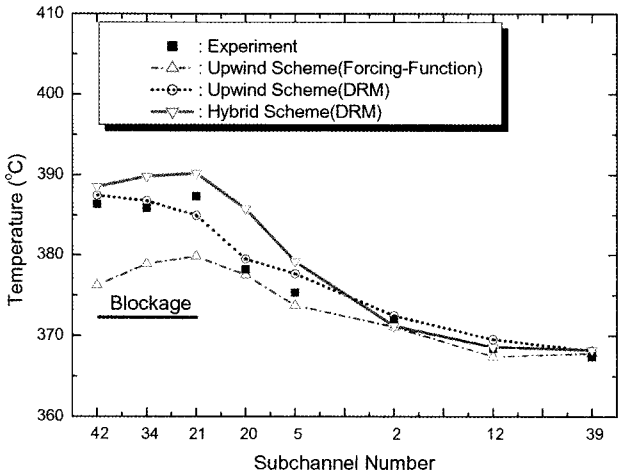

Fig. 6. The Calculation Results for ORNL High Flow Test with Blockage at Exit Region

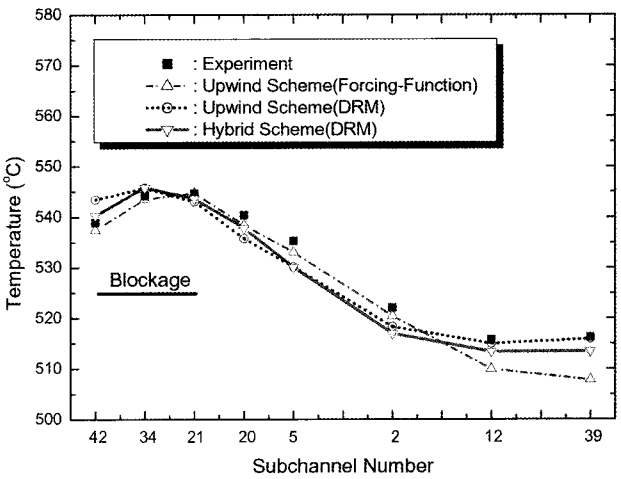

Fig. 7. The Calculation Results for ORNL Low Flow Test with Blockage at Exit Region

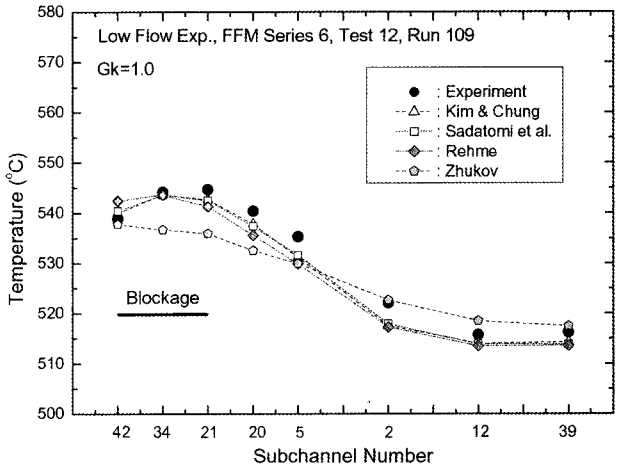

Fig. 8. Comparison of Turbulent Mixing Models for the Low-flow Case

profile shape and the magnitude in the blocked subchannel are predicted reasonably well.

The temperature distribution at the exit region is predicted reasonably with the wire forcing function, which is the original wire-wrap model. But the magnitude of the peak temperatures is significantly underestimated because the lateral flow rates are estimated in the wrong manner. The distributed resistance model with the upwind scheme gives much improved predictions but still fails to predict the location of the highest temperatures, especially at the boundary of the blockage plate. This is improved by employing the hybrid scheme in the low flow region. The overall temperature difference between the blocked region and the unblocked region, which amounts to about 20 °C, is calculated well with the hybrid scheme and the distributed resistance models.

Fig. 8 shows the effects of the turbulent mixing models

for the low-flow case. The Re number for this case is about 3800 and the Pe number is about 23. It is found that the Zhukov model is not applicable for the case and the correlations by Kim and Chung show slightly better results than do Rehme's correlations. The predictions made by Kim and Chung's model result in nearly the same temperature distributions as are reflected in the experimental data.

Fig. 9 and Fig. 10 compare the temperature distributions of the transverse direction at heights of 20 mm and 80 mm from the blockage plate for the 49 % central blockage with a 4 m/s inlet velocity. The MATRA-LMR-FB code overestimates the temperature trends at the height of 20 mm, especially for the center region of subchannel numbers 1 ~ 3; however, it accurately predicts the temperature at the height of 80 mm. The overestimation at the height of 20 mm may be caused by a discrepancy for the recirculation flow in the vicinity of the blockage. This overestimation in temperature prediction is closely related to the predicted distribution of velocity in the radial direction, as shown in Fig. 11. Fig. 11 also suggests that the characteristics of the recirculation flow are not calculated accurately, since the pressure drops in the transverse direction in the neighborhood of the blockage were not reflected realistically due to the absence of a grid spacer model in the MATRA-LMR-FB. In the present calculation, the form loss coefficient due to a grid in which a blockage is located has been calculated taking the area change into account. An appropriate model related to a grid spacer is required to simulate the exact recirculation due to a flow

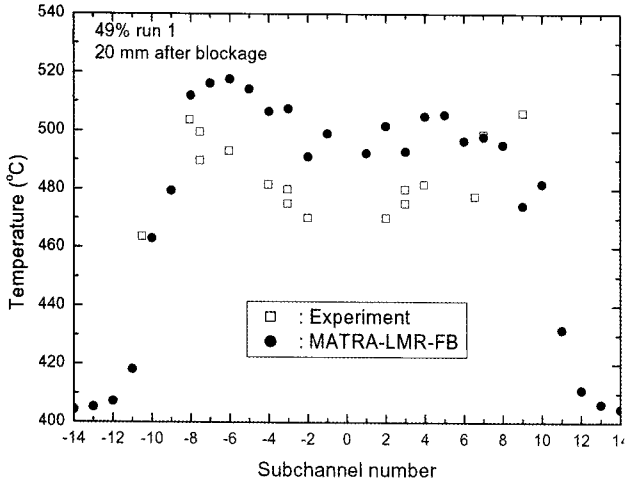

Fig. 9. Results at the Elevation of 20 mm after the Blockage for the Karlsruhe 49 % Central Blockage with the Velocity of 4 m/s

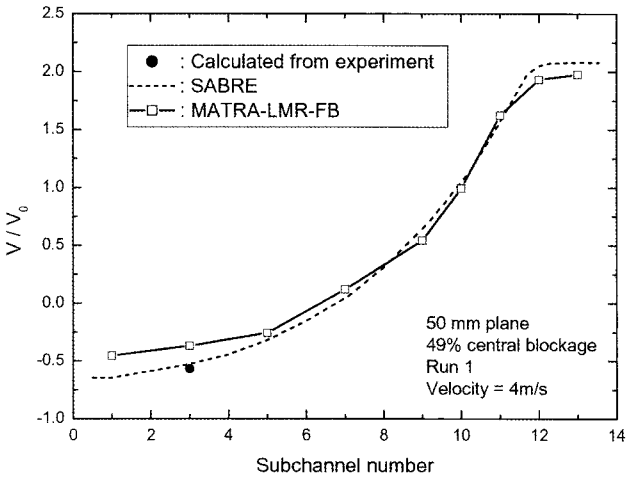

Fig. 11. Distribution of Radial Velocity at 50 mm after the Blockage for the Karlsruhe 49 % Central Blockage with the velocity of 4 m/s

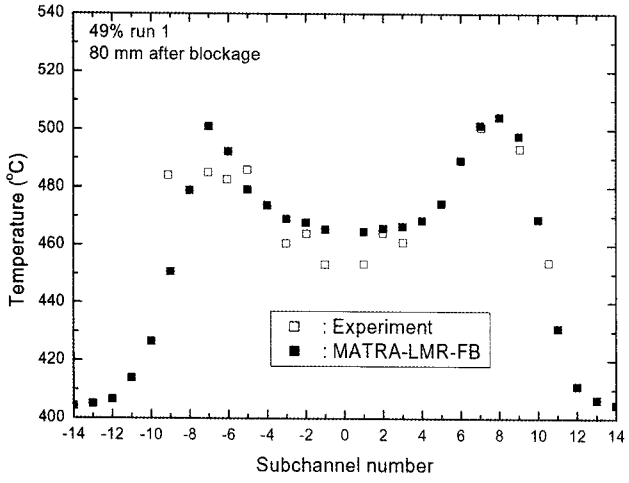

Fig. 10. Results at the Elevation of 80 mm after the Blockage for the Karlsruhe 49 % Central Blockage with the Velocity of 4 m/s

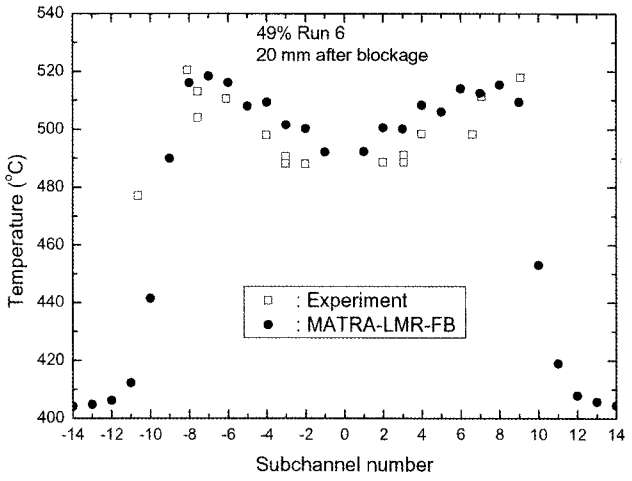

Fig. 12. Results at the Elevation of 20 mm after the Blockage for the Karlsruhe 49 % Central Blockage with the Velocity of 1 m/s

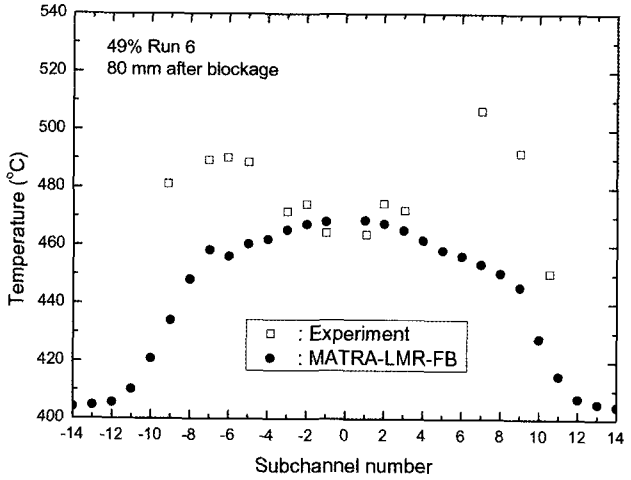

Fig. 13. Results at the Elevation of 80 mm after the Blockage for the Karlsruhe 49 % Central Blockage with the Velocity of 1 m/s

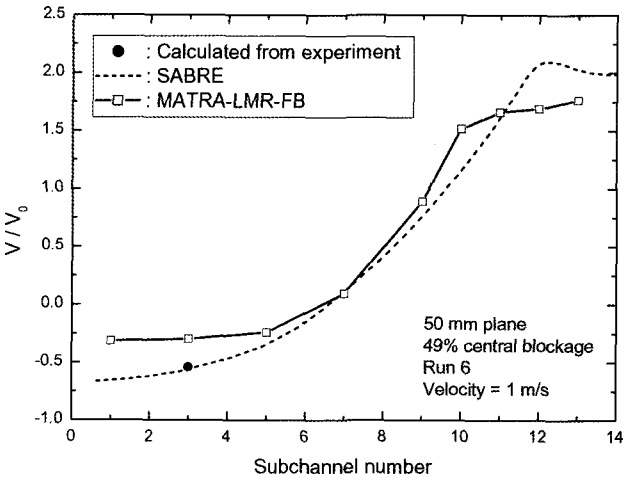

Fig. 15. Distribution of Radial Velocity at 50 mm after the Blockage for the Karlsruhe 49 % Central Blockage with the Velocity of 1 m/s

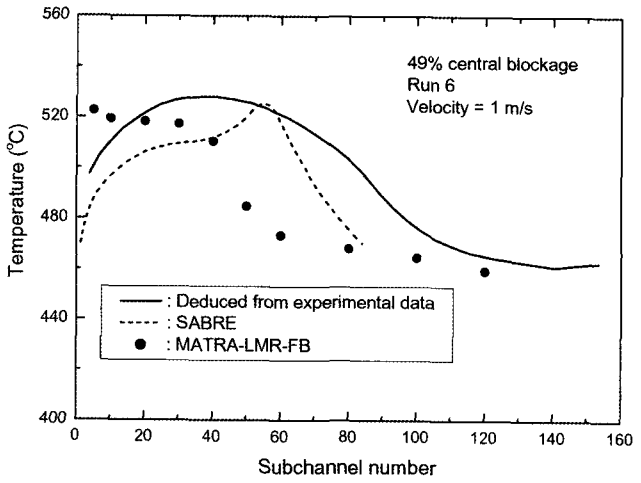

Fig. 14. Comparison of the Predicted Peak Temperature with the Experimental Results for the Karlsruhe 49 % Central Blockage with the Velocity of 1 m/s

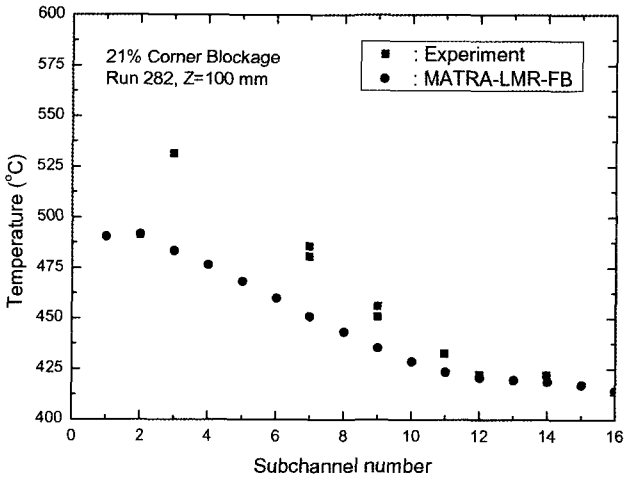

Fig. 16. Results at the Elevation of 100 mm after the Blockage for the Karlsruhe 21 % Corner Blockage with the Velocity of 1 m/s

blockage because the pressure drop coefficients should generally be differed according to Re number.

The simulation for the 49 % central blockage with a 1 m/s inlet velocity revealed results opposite to those in the former case, as shown in Fig. 12 and Fig. 13. The code yielded comparatively accurate results at the height of 20 mm while it underestimated the temperature at the height of 80 mm. The main cause of the underestimation is the active thermal mixing between the channels in the downstream of the blockage due to the small size of the recirculation region in the MATRA-LMR-FB calculation. The recirculation length can be estimated from the peak temperature distribution shown in Fig. 14. It is presumed that the small recirculation region is due to the inaccuracy in the transverse pressure drop that results in the velocity distribution shown in Fig. 15.

It is difficult to analyze cases where a blockage is formed at a corner because an asymmetric flow occurs in such cases. Fig. 16 shows the calculation results at the height of 100 mm from the blockage for the 21 % corner blockage with an inlet velocity of 1 m/s as compared to the experimental data, and Fig. 17 depicts the results for the 21 % corner blockage with an inlet velocity of 4 m/s. The temperature trends are underestimated, by comparison to the experimental data, because the length of the recirculation region is short when calculated by the MATRA-LMR-FB code.

The previous analyses for two typical subchannel

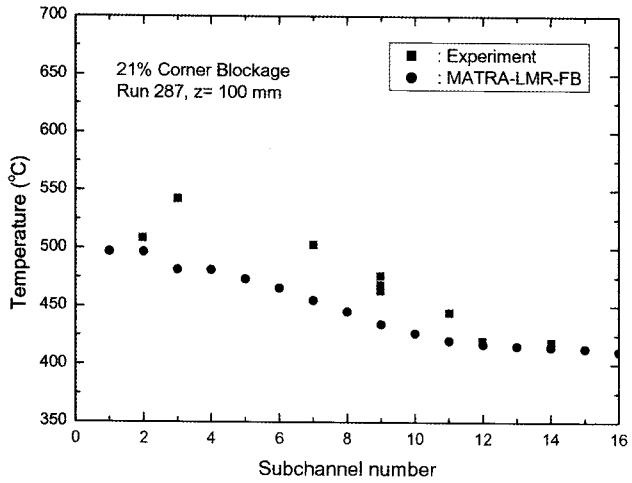

Fig. 17. Results at the Elevation of 100 mm after the Blockage for the Karlsruhe 21 % Corner Blockage with the Velocity of 4 m/s

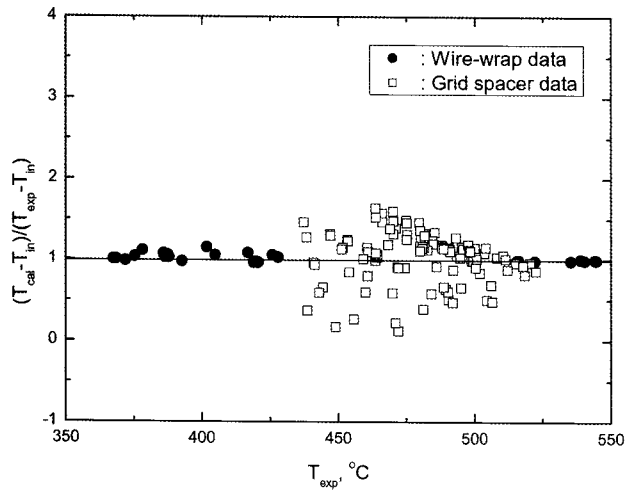

Fig. 18. Comparison of the Dimensionless Temperatures

types using the MATRA-LMR-FB code demonstrate its applicability for a blockage analysis. The results for the ORNL 19-pin experiments with wire spacers, in particular, agreed well with the experimental data when applying a distributed resistance model. However, the results for the Karlsruhe 169-pin tests with grid spacers were less accurate than the results with wire spacers as shown in Fig. 18, in which the calculated temperature increments that depend on the inlet temperature were compared to the experimental data. The mean and standard deviation for the dimensionless temperatures of the tests with the wire spacers are 1.013 and 0.047, while the values for the tests with grid spacers are 1.007 and 0.316.

4. CONCLUSIONS

The MATRA-LMR-FB code for the analysis of a subchannel blockage has been developed and evaluated using two groups of experimental data. The current version of the code was improved by the implementation of a distributed resistance model that accurately considers the effect of flow resistance on wire spacers, by the addition of a turbulent mixing model, and by the application of a hybrid scheme in low flow regions. ORNL 19-pin tests with wire spacers and Karlsruhe 169-pin tests with grid spacers were used to validate the code.

The calculations for the Karlsruhe 169-pin tests using the MATRA-LMR-FB code did not correctly simulate the characteristics of the recirculation flow at a short distance downstream from a blockage since the pressure drop in the transverse direction was not reflected realistically. Analysis revealed that the code requires an accurate model related to a grid spacer model. Results for the ORNL 19-pin tests using the code revealed acceptable accuracy, within a range of 5 °C, for the experimental data with a blockage. The standard deviation for the Karlsruhe 169-pin tests showed a large value of 0.316, while that for the ORNL 19-pin tests was 0.047. It is concluded that the MATRA-LMR-FB code can be used for the analysis of a subchannel blockage with wire spacers, but that a model related to grid spacers should be included.

NOMENCLATURE

A	subchannel flow area
A_R	rod surface area within the control volume
A_W	wire-wrap surface area within the control volume
a_x	directional velocity scale of the flow pulsation
b	shape factor for the length scale for the transverse flow pulsation
c	flow velocity
d	rod diameter
$[D_C]$	matrix for interchannel connection
D_h	hydraulic diameter of a subchannel
f	friction factor in rod bundle without wire wrap
F_R^A	axial component of the force exerted by the rod surface
F_R^L	lateral component of the force exerted by the rod surface
F_W^T	tangential component of the force exerted by the wire-wrap surface
F_W^N	normal component of the force exerted by the wire-wrap surface
g	gravitational constant
G	axial mass flux
h	enthalpy
K	form loss coefficient
K_G	lateral loss coefficient
l	distance between the center of the two adjacent subchannels
m	axial flow rate

p pressure
Pe turbulent Peclet number
Pr turbulent Prandtl number
S gap size
St_g gap Stanton number
Str Strouhal's number
t time
u axial velocity
u' fluctuating component of axial velocity
v transverse velocity
v' fluctuating transverse velocity
V volume of a control volume
w lateral flow rate
w' fluctuating lateral flow rate
x coordinate of axial direction
z_{FP} hypothetical path length of flow pulsation

Greek

α constant for friction factor
β turbulent mixing coefficient, constant for friction factor
δ distance between the center of two adjacent subchannels
Δ node size
ε_H eddy diffusivity for energy
ϕ angle between the wire-wrap and fuel rod
γ empirical constant in Eq. (16)
θ angle between the flow and the fuel rod
ρ density
ω wire-wrap position

Subscripts

FP flow pulsation
i subchannel i
ij from subchannel i to subchannel j, between subchannels i and j
j subchannel j
N Normal direction to wall surface
T Tangential direction to wall surface

REFERENCES

[1] Kim, W. S., Kim, Y. G. and Kim, Y. J., "A Subchannel Analysis Code MATRA-LMR for Wire-Wrapped LMR subassembly," Annals of Nuclear Energy, 29, 303, 2002.
[2] Stewart, C. W., Wheeler, C. L., Cena, R. J., McMonagle, C. Cuta, A. J. M. and Trent, D. S., "COBRA-IV : The model and the method," BNWL-2214, Pacific Northwest Laboratoies, 1977.
[3] Ninokata, H., Efthimiadis, A. and Todreas, N. E., "Distributed Resistance Modeling of wire-wrapped Rod Bundles," Nucl. Eng. Des., 104, 93, 1987.
[4] Davis, A. L. et al., " SABRE I –A computer program for the calculation of three dimensional flows in rod clusters," AEEW-R 1057, 1979.
[5] Kim, S. and Chung, B. J., "A scale analysis of the mixing rate for various Prandtl number flow fields in rod bundles," Nucl. Eng. Des., 205, 281, 2001.
[6] Sadatomi, M., Kawahara, A. and Sato, Y., "Prediction of the single-phase turbulent mixing rate between two parallel subchannels using a subchannel geometry factor," Nucl. Eng. Des., 162, 245, 1996.
[7] Rheme, K., "The structure of turbulence in rod bundles and the implications on natural mixing between the subchannels," Int. J. Heat Mass Transfer, 35, 567, 1992.
[8] Zhukov, A. V., Kirilov, P. L., Sorokin, A. P. and Matjukhin, N. M., "Transverse turbulent momentum and energy exchange in the channels of complicated form," Proc. Heat Transfer, Brighton, Vol. 4, p. 327, 1994.
[9] Kays, W. M., "Turbulent Prandtl Number-Where Are We ?," J. Heat Transfer, 116, 284, 1994.
[10] Ha, K. S. et al., "Wire-wrap models for Subchannel Blockage Analysis," J. Korean Nucl. Soc., 36, 2, 2004.
[11] Suh, K. Y., and Todreas, N. E., "An Experimental correlation at crossflow pressure drop for triangular array wire-wrapped rod assemblies," Nucl. Technol., 76. 229-240, 1987.
[12] Patankar, S. V., "Numerical Heat Transfer and Fluid Flow," hemisphere publishing corp., 83-96, 1979.
[13] Jeong, H. Y. et al., "Modeling of flow blockage in a liquid metal-cooled reactor subassembly with a subchannel analysis code," Nucl. Technol., 149, 1, 2005.
[14] Fontana, M. H. et al., "Temperature distribution in the duct wall and at the exit of a 19-rod simulated LMFBR fuel assembly (FFM Bundle 2A)," Nucl. Technol., 24, 176-200, 1974.
[15] Domanus, H. M., Shah, V. L. and Sha, W. T., "Applications of the COMMIX code using the porous medium-formulation," Nucl. Energ. Des., 62, 81-100, 1980.
[16] Huber, F. and Peppler, W., "Summary and Implications of Out-of-pile Investigations of Local Cooling Distributions in LMFBR Subassembly Geometry under Single-phase and Boiling Conditions," KfK 3927, Kernforschungszentrun Karlsruhe, 1985.